Article | Received 22 June 2026; Revised 20 August 2026; Accepted 28 August 2026; Published 10 September 2026
https://doi.org/10.55092/la20260010

Photocatalytic self-cleaning and recyclable AuNBPs@TiO_2 SERS chip for trace detection and *in situ* monitoring of methylene blue degradation

Yuanyuan Yao[1,2,*], Jiani Li[2], Xianqi Fang[2], Aijie Yu[3,*] and Baohong Liu[1,*]

[1] Department of Chemistry, Shanghai Stomatological Hospital, School of Pharmacy, Institute of Biomedical Sciences, Fudan University, Shanghai, China
[2] Provincial Key Laboratory of Multimodal Perceiving and Intelligent Systems, Engineering Research Center of Intelligent Human Health Situation Awareness of Zhejiang Province, Jiaxing Key Laboratory of Molecular Recognition and Sensing, College of Biological and Chemical Engineering, Jiaxing University, Jiaxing, China
[3] Department of Geriatrics, Putuo Hospital, Shanghai University of Traditional Chinese Medicine, Shanghai, China

* Correspondence authors; E-mails: yaoyy@zjxu.edu.cn (Y.Y.); yuaijie2022@126.com (A.Y.); bhliu@fudan.edu.cn (B.L.).

Highlights:

- The AuNBPs@TiO_2 chip integrates sensitive SERS detection with photocatalytic self-cleaning.
- SERS chip enables in situ monitoring of MB photodegradation with a 3.3 nM detection limit.
- The recyclable chip maintains > 95% degradation efficiency and 89.5% SERS signal after 8 cycles.

Abstract: Recyclable surface-enhanced Raman scattering (SERS) substrates integrating high sensitivity with effective photocatalytic self-cleaning capability are highly desirable for sustainable pollutant analysis, yet maintaining stable SERS activity during repeated photocatalytic regeneration remains challenging. Herein, a photocatalytic self-cleaning AuNBPs@TiO_2 SERS chip was constructed by integrating plasmonic gold nanobipyramids with a photocatalytic TiO_2 shell. By regulating the hydrolytic coating process, a uniform TiO_2 shell with an optimized thickness of approximately 10 nm was obtained, providing a balance between SERS enhancement and photocatalytic activity. Using methylene blue (MB) as a model organic pollutant, the chip exhibited a wide linear detection range from 10 nM to 1 mM with a low limit of detection of 3.3 nM. The intra-chip and inter-batch relative standard deviations were below 10%, indicating good uniformity and reproducibility. Furthermore, time-dependent SERS spectra enabled *in situ* monitoring of MB photodegradation under xenon lamp irradiation, with degradation efficiencies exceeding 95% within 90 min for MB concentrations of 10^{-4}–10^{-6} M. Independent UV-vis measurements further confirmed MB degradation, showing an 81.91% decrease after 90 min for 10^{-5} M MB. After 12 cycles, the chip retained approximately 72% of its initial SERS signal while maintaining a degradation efficiency above 90%. The AuNBPs@TiO_2 chip offers a reusable SERS platform for sensitive MB

detection and *in situ* monitoring of photocatalytic degradation, demonstrating the feasibility of integrating trace detection, photocatalytic regeneration, and repeated use within a single analytical platform.

Keywords: surface-enhanced Raman scattering; self-cleaning; photocatalytic degradation; *in situ* monitoring; organic pollutant

1. Introduction

Surface-enhanced Raman scattering (SERS) has emerged as a powerful analytical technique for qualitative and quantitative detection in environmental monitoring, food safety, and biomedical applications owing to its ultrahigh sensitivity, molecular fingerprint capability, and suitability for trace analysis [1–3]. However, conventional noble metal-based SERS substrates are generally limited by poor reusability because adsorbed analytes are difficult to remove completely after measurement, resulting in increased analytical cost and potential secondary contamination [4–6]. Self-cleaning SERS substrates based on semiconductor photocatalysis provide an effective strategy for substrate regeneration by degrading adsorbed molecules under light irradiation [7,8]. Nevertheless, pure semiconductor substrates generally exhibited insufficient SERS enhancement, whereas semiconductor/metal composite SERS substrates may suffer from signal degradation and poor cycling stability due to nanoparticle aggregation, surface modification, or structural instability during reused [9–11]. Therefore, the development of recyclable SERS substrates that integrate high sensitivity, efficient photocatalytic performance, and reliable cycling stability is essential for sustainable analytical applications.

Semiconductor/metal composite SERS substrates provide an effective strategy for integrating the localized surface plasmon resonance (LSPR) enhancement of noble metals with the photocatalytic functionality of semiconductors [12,13]. Noble metal nanostructures, such as Au and Ag, provide strong electromagnetic enhancement for SERS detection, whereas semiconductor components enable photoinduced charge separation and surface redox reactions for the degradation of adsorbed molecules. This synergistic integration enables both ultrasensitive detection and *in situ* self-regeneration of SERS activity. Recent studies have increasingly validated the effectiveness of semiconductor/metal composite substrates for recyclable SERS detection. For instance, Liu *et al.* constructed three-dimensional flower-like MoS_2/Ag@rGO nanocomposites for trace detection of 17β-estradiol in environmental water and demonstrated up to eight self-cleaning reuse cycles [14]. Kumar *et al.* developed an Ag-modified Mn_2O_3 substrate that retained 92% of SERS activity after five regeneration cycles for furazolidone detection [15]. Zhai *et al.* developed Au-MoS_2 nanocomposites for ultrasensitive crystal violet detection over a concentration range of 10^{-5}–10^{-16} M, achieving 99.64% photocatalytic degradation after 240 min of illumination and seven reuse cycles [16]. Au/TiO_2 [17], Ag/TiO_2 [18], and hollow Au@TiO_2 core-shell [19] SERS platforms have further demonstrated the feasibility of coupling plasmonic SERS enhancement with light-triggered photocatalytic regeneration. However, simultaneously maintaining sufficient SERS sensitivity, effective photocatalytic regeneration, and reproducible performance over repeated cycles remains challenging. Such integrated platforms are also relevant to environmental toxicology and exposure assessment, where trace contaminants may need to be detected and monitored in complex environmental or biological matrices. Consequently, rational control of the plasmonic nanostructure and semiconductor shell is essential for balancing electromagnetic enhancement with photocatalytic functionality and recyclability.

Herein, we developed a photocatalytic self-cleaning and recyclable AuNBPs@TiO_2 core-shell SERS chip by integrating the anisotropic of gold nanobipyramids (AuNBPs) with a photocatalytic TiO_2 shell. The high-curvature tips and longitudinal plasmonic mode of AuNBPs provide localized electromagnetic-field enhancement for sensitive SERS detection. Meanwhile, the TiO_2 shell enables photocatalytic degradation of adsorbed methylene blue (MB), which was selected as a model organic pollutant. The TiO_2 shell thickness was carefully regulated to balance the plasmonic SERS response with photocatalytic activity. This proposed AuNBPs@TiO_2 SERS chip enables integrated trace detection, real-time *in situ* monitoring of organic pollutant degradation, and repeated self-cleaning reuse within a single SERS chip.

2. Experimental section

2.1. Chemicals and reagents

Hydrogen tetrachloroaurate (III) tetrahydrate ($HAuCl_4 \cdot 4H_2O$, 48%–50%), trisodium citrate (99%), silver nitrate ($AgNO_3$, 99.8%), hydrochloric acid (HCl, 36%–38%), sodium bicarbonate ($NaHCO_3$, 99.5%), and methylene blue (98%) were obtained from Sinopharm Chemical Reagent Co., Ltd. Cetyltrimethy lammonium bromide (CTAB, 98%) and cetyltrimethy lammonium chloride (CTAC, 98%) were purchased from Sangon Biotech (Shanghai) Co., Ltd. Sodium borohydride ($NaBH_4$, 98%) and titanium trichloride ($TiCl_3$, 15%) were purchased from Aladdin Reagent Co., Ltd. Silicon wafers (1 cm × 1 cm) were procured from Jingxin Electronics Technology Co., Ltd. Ascorbic acid (AA, 99%), fetal bovine serum (FBS) and phosphate-buffered saline (PBS) were purchased from Sigma-Aldrich (USA). Ultrapure water with a resistivity of 18.25 MΩ·cm was used throughout all experiments.

2.2. Apparatus

Transmission electron microscopy (TEM) images were obtained using a Talos F200X transmission electron microscope (Thermo Scientific, USA). Scanning electron microscopy (SEM) images were acquired using an Apreo S HiVac scanning electron microscope (Thermo Scientific, USA). Energy-dispersive X-ray spectroscopy (EDS) analysis was performed using an Oxford X-Max N spectrometer (Oxford Instruments, UK). UV-vis absorption spectra were recorded on a UV-2700 spectrophotometer (Shimadzu, Japan). SERS measurements were carried out using a portable Raman spectrometer (SEED 3000, Ruhai Optoelectronic Technology Co., Ltd.) with a 785 nm excitation laser. Photocatalytic degradation experiments were conducted using a xenon lamp light source (PLS-SXE300, Beijing Bofeilai Technology Co., Ltd., China). A constant-temperature oil bath (HBC 10, IKA, Germany), vortex mixer (DU-3GW, WIGGENS, Germany), high-speed refrigerated centrifuge (H1850R, Hunan Xiangyi Laboratory Instrument Development Co., Ltd., China), and ultrasonic cleaner (KQ-500DE, Kunshan Ultrasonic Instruments Co., Ltd., China) were used for sample preparation and processing.

2.3. Synthesis of AuNBPs

AuNBPs were prepared using the thermally induced seed-mediated growth method with slight modifications to a previously reported procedure [20]. Briefly, the gold seed solution was prepared by rapidly injecting 0.6 mL of freshly prepared ice-cold $NaBH_4$ solution (0.01 M) into a mixed solution

containing CTAC (10 mL, 0.1 M), trisodium citrate (0.5 mL, 0.01 M), and $HAuCl_4$ (0.5 mL, 0.01 M) under vigorous stirring. After stirring for 10 min, the mixture was transferred to an 80 °C oil bath for 90 min. The resulting seed solution was cooled to room temperature and stored at 4 °C. For AuNBPs growth, CTAB (3.645 g) was dissolved in 100 mL of deionized water under stirring at 55 °C. Subsequently, $HAuCl_4$ (2 mL, 10 mM), $AgNO_3$ (1 mL, 10 mM), and HCl (2 mL, 1.0 M) were sequentially added to the CTAB solution and mixed thoroughly. Then, 0.8 mL of AA (0.1 M) was rapidly introduced, causing the solution color changed from orange-yellow to colorless. Finally, 2.5 mL of the gold seed solution was added, and the mixture gradually turned light purple. After gentle stirring for 5 min, the solution was incubated overnight in a 30 °C water bath. The obtained AuNBPs were purified by centrifugation at 6500 rpm for 8 min. The purified AuNBPs were finally dispersed in 10 mL of CTAC solution (0.08 M) and stored in the dark before further use. The morphology and optical properties of the AuNBPs were characterized by TEM and UV-vis spectroscopy, respectively.

2.4. Preparation of AuNBPs@TiO_2 nanocomposites

AuNBPs@TiO_2 core-shell nanocomposites were synthesized using a hydrolytic coating method. Briefly, 100 μL of $TiCl_3$ aqueous solution was added to deionized water (4 mL, 18.25 MΩ·cm). The mixture was stirred in the dark for 10 min to allow $TiCl_3$ hydrolysis, resulting in a pale purple solution. Subsequently, different volumes (350, 400, 450, 500, and 600 μL) of $NaHCO_3$ solution (1.0 M) were slowly added dropwise under continuous stirring, and the solution color gradually changed to dark blue. Then, 1 mL of AuNBPs solution was rapidly introduced into the mixture and reacted in the dark for 60 min. After the reaction, the products were collected by centrifugation at 6500 rpm for 8 min, washed three times with anhydrous ethanol to remove residual $TiCl_3$ and $NaHCO_3$, and finally redispersed in 5 mL of anhydrous ethanol. The obtained AuNBPs@TiO_2 nanocomposites were stored in the dark before further use. The core-shell morphology of AuNBPs@TiO_2 was characterized by TEM, while elemental composition and distribution were analyzed by EDS. UV-vis spectroscopy was used to evaluate the optical properties of the nanocomposites.

2.5. Preparation and performance of SERS chip

Single-crystal silicon wafers (1 cm × 1 cm) were used as chip substrates. Prior to use, the wafers were sequentially ultrasonically cleaned in acetone, anhydrous ethanol, and ultrapure water for 10 min respectively to remove surface contaminants and organic residues. The prepared AuNBPs@TiO_2 nanocomposites dispersions were adjusted to different concentrations, including 2, 4, 6, 8, 10, 12, and 14 nM. Subsequently, 20 μL of each concentrated AuNBPs@TiO_2 was dropped onto the pretreated silicon wafer surface and dried at room temperature to obtain the AuNBPs@TiO_2 SERS chips. For SERS measurements, 5 μL of MB solution at different concentrations was added onto the chip surface. After drying at room temperature, SERS spectra were collected using a portable Raman spectrometer equipped with a 785 nm excitation laser. The laser power, integration time, and spectral range were set to 65 mW, 2000 ms, and 200–2000 cm^{-1}, respectively.

To further evaluate the uniformity of the drop-cast SERS chip, SERS mapping was performed over a 1 × 1 cm^2 region using a 10 × 10 grid, yielding a total of 100 measurement sites. Spectra were collected from all sites under identical acquisition conditions, and the intensity of the characteristic MB band at

1624 cm^{-1} was extracted to construct a two-dimensional SERS intensity map. The relative standard deviation (RSD) of the intensities obtained from the 100 measurement sites was calculated to evaluate the spatial reproducibility of the chip.

2.6. In situ monitoring of MB photocatalytic degradation

20 μL of 10 nM concentrated AuNBPs@TiO_2 dispersion was dropped onto a silicon wafer and dried at room temperature to prepare the SERS chip. Subsequently, 10 μL of MB solution (10^{-5} M) was added onto the chip and dried naturally. A fixed detection spot was marked, and the initial SERS spectrum was recorded as t_0. The chip was then placed directly under a xenon lamp at a distance of 15 cm, with the lamp current set to 22.3 mA. SERS spectra were collected from the same detection spot every 15 min until 90 min to monitor the photocatalytic degradation process. The same procedure was applied to MB solutions with initial concentrations of 10^{-4}, 10^{-5}, and 10^{-6} M to evaluate the concentration-dependent evolution of the SERS response during photocatalytic irradiation.

To independently verify MB photodegradation, UV-vis absorption spectroscopy was performed under the same xenon-lamp irradiation conditions. A 10^{-5} M MB solution in the presence of the AuNBPs@TiO_2 chip was irradiated, and UV-vis spectra were recorded at 0, 15, 30, 45, 60, 75, and 90 min. The characteristic absorption band of MB at approximately 666 nm was used to monitor changes in the bulk-phase MB concentration. A dark control experiment was performed in parallel using the AuNBPs@TiO_2 chip without xenon-lamp irradiation. UV-vis spectra were recorded at the same time intervals to evaluate changes.

2.7. Cycling stability of SERS chips

To evaluate the photocatalytic self-cleaning and recycling performance of the AuNBPs@TiO_2 SERS chip, 10 μL of MB solution (10^{-5} M) was deposited onto the SERS substrate and dried at room temperature. The initial SERS spectrum was recorded immediately after MB deposition and defined as t_0. The chip was irradiated under a xenon lamp for 90 min to induce photocatalytic degradation, and the residual SERS signal was recorded as t_{90}. The degradation process was defined as one cycle and was repeated 12 times to assess the long-term recyclability of the SERS chip. After 12 detection-regeneration cycles, the chip was further characterized by SEM to evaluate changes in particle distribution and surface morphology induced by repeated irradiation and washing.

2.8. Analysis of MB in complex biological and food matrices

To evaluate the applicability of the proposed SERS chip in complex matrices, FBS and fish muscle samples were used as representative biological and food matrices, respectively. FBS was diluted to 10% (v/v) with PBS (pH 7.4), and MB was spiked at final concentrations of 0.01, 1.00, and 100.00 μM. For fish muscle samples, 1.0 g of homogenized fish muscle was spiked with MB at the same concentrations, followed by addition of 9.0 mL PBS (pH 7.4). After ultrasonic extraction and centrifugation, the supernatant was collected for SERS analysis, and the analytical performance was evaluated based on recovery and RSD.

3. Results and discussion

3.1. Design of the AuNBPs@TiO_2 SERS chip

The fabrication process and photocatalytic self-cleaning mechanism of the AuNBPs@TiO_2 SERS chip were schematically illustrated in Figure 1. AuNBPs@TiO_2 core-shell nanocomposites were constructed by combining the seed-mediated synthesis of AuNBPs with subsequent hydrolytic coating of TiO_2. The obtained AuNBPs@TiO_2 nanocomposites were deposited onto silicon wafers to construct a recyclable SERS chip capable of integrating sensitive detection, *in situ* monitoring of photocatalytic degradation, and light-triggered regeneration within a single platform. AuNBPs were employed as the plasmonic core which provided "lightning rod" effect and strong localized electromagnetic fields, thereby contributing to enhanced SERS sensitivity [21,22]. TiO_2 shell serves as the photocatalytic component of the core-shell structure. Under xenon-lamp irradiation, TiO_2 generated photogenerated electron-hole pairs. The photogenerated holes can oxidize surface-adsorbed H_2O or OH^- to produce reactive hydroxyl radicals (·OH), while electrons can reduce dissolved O_2 to generate superoxide radicals ($\cdot O_2^-$). These reactive oxygen species, together with photogenerated holes, promote the oxidative degradation of MB adsorbed on the chip surface [23,24]. In addition, the favorable band alignment between TiO_2 and Au facilitates electron transfer from TiO_2 to Au, forming a Schottky junction that suppresses charge recombination and further enhances photocatalytic efficiency [25,26]. Thus, the AuNBPs@TiO_2 core-shell architecture combines the plasmonic SERS response of AuNBPs with the photocatalytic functionality of TiO_2, enabling trace MB detection, time-resolved monitoring of MB photocatalytic degradation, and repeated light-triggered regeneration of the SERS chip.

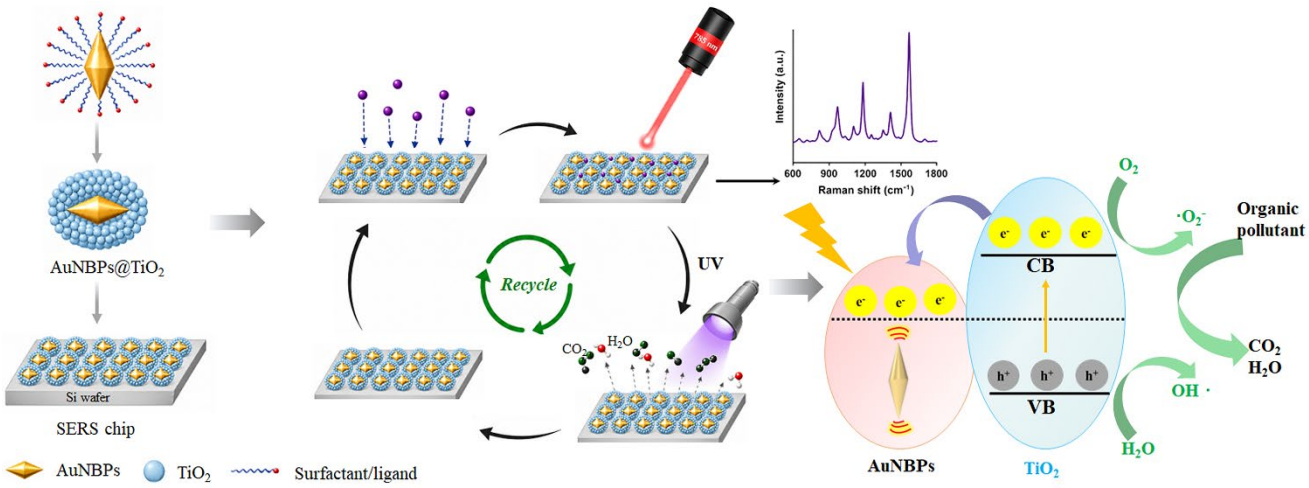

Figure 1. Schematic illustration of the fabrication process and photocatalytic self-cleaning mechanism of the AuNBPs@TiO_2 SERS chip.

3.2. Characterization of AuNBPs@TiO_2 nanocomposite

The morphology and optical properties of AuNBPs@TiO_2 nanocomposite were characterized by UV-vis spectroscopy, TEM, and EDS analysis. As shown in Figure 2a, the AuNBPs exhibited a characteristic longitudinal LSPR band at 724 nm, corresponding to their anisotropic bipyramidal morphology. After TiO_2 coating, the LSPR band shifted to 755 nm, attributing to the high refractive index TiO_2 shell surrounding

the AuNBPs core. TEM characterization further confirmed the formation of the core-shell nanocomposites. As shown in Figure 2d, the AuNBPs core retained a well-defined bipyramidal morphology with sharp tips, while a uniform TiO_2 shell was coated on the AuNBPs surface, indicating the successful synthesis of AuNBPs@TiO_2 core-shell nanocomposites. Statistical analysis of more than 50 particles revealed that the AuNBPs core had an average longitudinal length of 111.1 ± 1.2 nm and transverse width of 44.4 ± 2.1 nm, corresponding to an aspect ratio of approximately 2.50. The average TiO_2 shell thickness was measured to be 11.1 ± 1.0 nm.

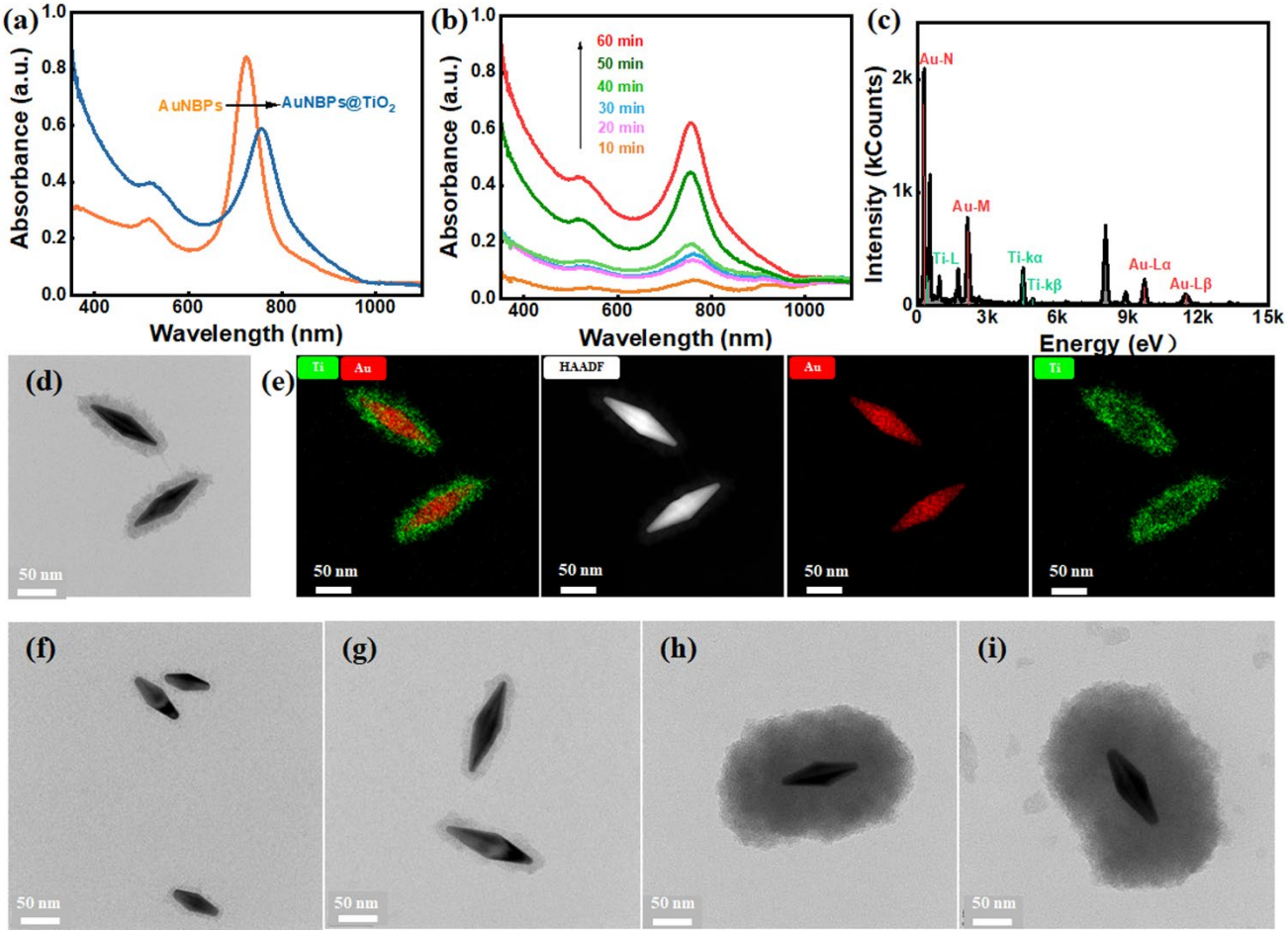

Figure 2. Characterization of AuNBPs@TiO_2 nanocomposites. **(a)** Extinction spectra of AuNBPs and AuNBPs@TiO_2; **(b)** Extinction spectra of AuNBPs@TiO_2 during TiO_2 shell growth; **(c)** EDS spectrum of AuNBPs@TiO_2; **(d)** TEM image of AuNBPs@TiO_2; **(e)** Elemental mapping images of AuNBPs@TiO_2; (**f–i**) TEM images of AuNBPs@TiO_2 prepared with different $NaHCO_3$ addition volumes: **(f)** 400 μL, **(g)** 450 μL, **(h)** 500 μL, and **(i)** 600 μL.

The elemental mapping of AuNBPs@TiO_2 were further verified in Figure 2e. The Au signal was mainly localized in the bipyramidal core region, whereas Ti and O were uniformly distributed around the Au core, consistent with the TiO_2 shell observed in the TEM images. The corresponding EDS spectrum showed the characteristic signals associated with Au and Ti, further supporting the successful formation of the AuNBPs@TiO_2 nanocomposites (Figure 2c). TEM images obtained under different $NaHCO_3$ volumes (Figure 2f–i) further demonstrate that the TiO_2 shell thickness can be effectively regulated while preserving the bipyramidal Au core.

3.3. Optimization of SERS chip fabrication parameters

3.3.1. Optimization of TiO_2 shell thickness

The TiO_2 shell thickness is a key parameter affecting both the SERS sensitivity and photocatalytic self-cleaning performance of the AuNBPs@TiO_2 chip. A thin TiO_2 shell may provide insufficient photocatalytic activity and limited protection of the AuNBPs core, whereas an excessively thick shell can increase the distance between analyte molecules and the plasmonic AuNBPs surface, thereby weakening the electromagnetic enhancement and decreasing SERS sensitivity. Therefore, precise regulation of the TiO_2 shell thickness is essential for balancing SERS sensitivity and photocatalytic regeneration.

The TiO_2 shell thickness was optimized by varying the reaction time and $NaHCO_3$ dosage during the hydrolytic coating process. As shown in Figure 2b, the extinction spectra of AuNBPs@TiO_2 gradually evolved with increasing reaction time from 10 to 60 min. At shorter reaction times, the extinction band was relatively broad, suggesting incomplete or nonuniform TiO_2 coating. With increasing reaction time, the spectral profile gradually became sharper and more stable. After 60 min, the extinction peak stabilized at approximately 755 nm, indicating the formation of uniform TiO_2 shell. The absorbance at 755 nm was further plotted as a function of reaction time (Figure S1). The absorbance increased progressively from 10 to 60 min and then tended to plateau, suggesting that the hydrolysis and shell growth process approached saturation after 60 min. Therefore, 60 min was selected as the optimal reaction time for subsequent preparation.

In addition, the $NaHCO_3$ dosage was further optimized due to its important role in regulating $TiCl_3$ hydrolysis by the modulating the reaction pH and hydrolysis rate, thereby influencing the growth and morphology of the TiO_2 shell. TEM images of AuNBPs@TiO_2 prepared using different $NaHCO_3$ volumes were shown in Figure 2f–i. At 400 μL of $NaHCO_3$, the TiO_2 shell was thin, discontinuous, and irregular, with a thickness of only 2–3 nm (Figure 2f). The incomplete coating may be attributed to insufficient pH regulation during $TiCl_3$ hydrolysis, which hindered uniform TiO_2 growth on the AuNBPs surface. With the increase of the $NaHCO_3$ volume to 450 μL, a uniform TiO_2 shell with a thickness of approximately 10–13 nm was exhibited (Figure 2g). When the $NaHCO_3$ volume was further increased to 500 or 600 μL, the TiO_2 shell became excessively thick, reaching approximately 60–70 nm (Figure 2h,i). Such overgrowth may reduce molecular accessibility to the plasmonic surface and attenuate the SERS enhancement.

The influence of $NaHCO_3$ dosage on SERS performance was further evaluated using MB (10^{-3} M) as a model molecule. The SERS intensity of the Raman peak at 1624 cm^{-1}, assigned to the C = C skeletal vibration, was compared for substrates prepared with different $NaHCO_3$ volumes (Figure 3a,b). As shown in Figure 3b, the SERS chip prepared with 450 μL of $NaHCO_3$ exhibited the strongest SERS response. The signal intensity was approximately 47% higher than that obtained with 400 μL of $NaHCO_3$. When the $NaHCO_3$ volume was increased to 500 μL, the signal decreased to 72% of that at 450 μL, and further decreased to 41% at 600 μL. This decline mainly attributed to the excessive TiO_2 shell thickness, which hinders MB access to the plasmonic hot spots and attenuates the electromagnetic enhancement. Therefore, 450 μL of $NaHCO_3$ was selected as the optimal volume for subsequent experiments. Under these conditions, the AuNBPs@TiO_2 nanocomposites possessed a uniform TiO_2 shell with suitable thickness, providing a favorable balance between SERS enhancement and photocatalytic self-cleaning capability.

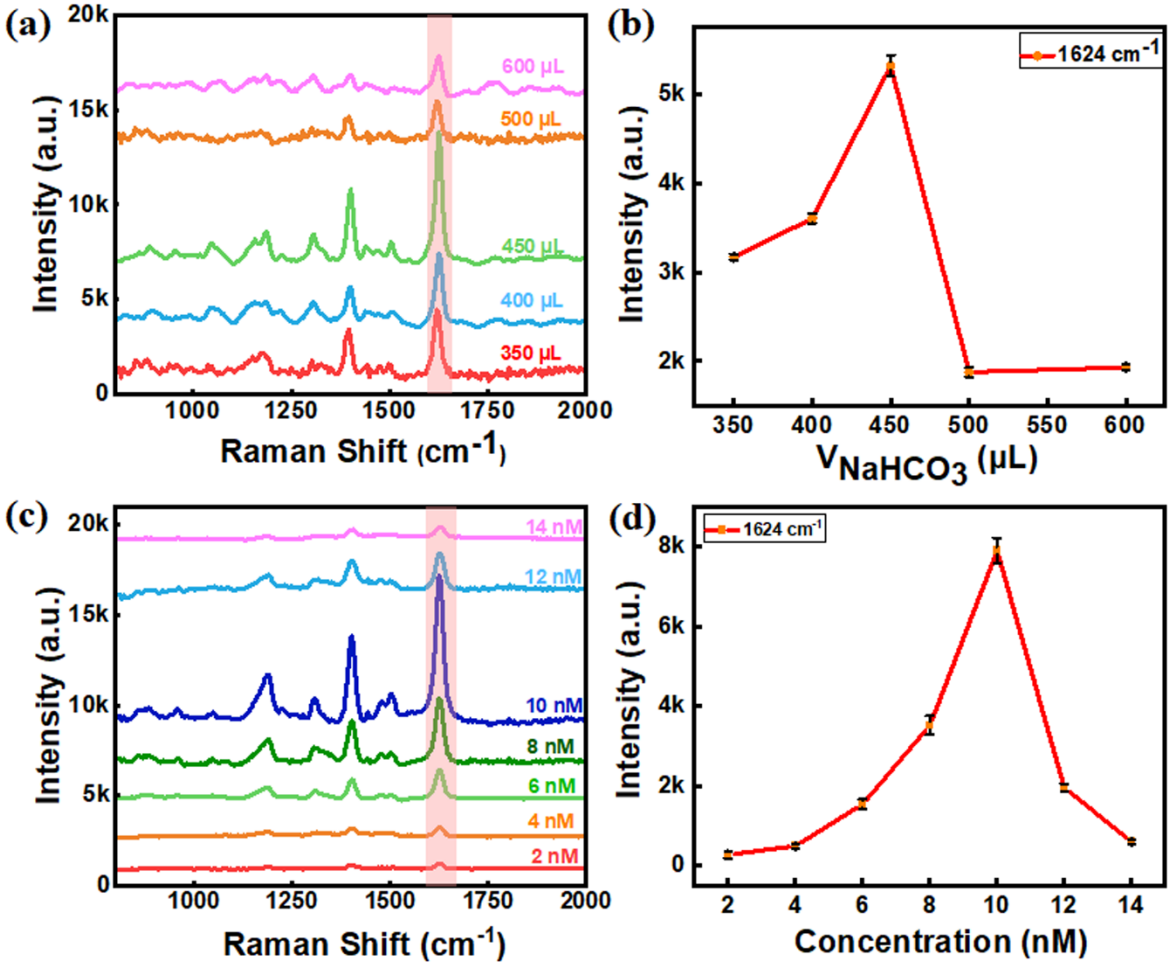

Figure 3. Optimization of fabrication parameters for the AuNBPs@TiO_2 SERS chip. **(a)** SERS spectra of 10^{-3} M MB on AuNBPs@TiO_2 chips prepared with different $NaHCO_3$ volumes; **(b)** Corresponding SERS intensity at 1624 cm^{-1} for different $NaHCO_3$ volumes; **(c)** SERS spectra of 10^{-3} M MB on AuNBPs@TiO_2 chips prepared with different AuNBPs@TiO_2 concentrations; **(d)** Corresponding SERS intensity at 1624 cm^{-1} for different AuNBPs@TiO_2 concentration.

3.3.2. Optimization of AuNBPs@TiO_2 concentration

The SERS performance of the fabricated AuNBPs@TiO_2 SERS chip was further optimized by varying the concentration of AuNBPs@TiO_2 nanomaterial from 2 nM to 14 nM (Figure 3c,d). As shown in Figure 3d, the SERS intensity of characteristic MB peak at 1624 cm^{-1} initially increased with the increase of AuNBPs@TiO_2 concentration and reached the maximum at 10 nM, followed by a gradual decrease at higher concentrations. At relatively low concentrations, the limited surface coverage of AuNBPs@TiO_2 reduces the number of plasmonic active nanostructures available within the laser sampling area and decreases the probability of interaction between MB molecules and the SERS-active surface. Increasing the nanocomposite concentration improves surface coverage and consequently enhances the overall SERS response. However, excessive deposition at higher concentrations may lead to increased particle aggregation and nonuniform stacking, which can alter the local plasmonic environment and reduce the accessibility of MB molecules to effective SERS-active regions [27,28]. Therefore, 10 nM of AuNBPs@TiO_2 nanocomposites was selected as the optimal concentration for subsequent SERS chip fabrication.

3.4. SERS performance of AuNBPs@TiO_2 chip

To evaluate the feasibility of AuNBPs@TiO_2 SERS chip. SERS spectra of 1.0 M MB solution, and 10^{-3} M MB on the AuNBPs SERS substrate and AuNBPs@TiO_2 SERS substrate were performed in Figure 4a. In the absence of a SERS substrate, the characteristic Raman peak of MB at 1624 cm^{-1} was barely discernible even at a high concentration of 1.0 M. In contrast, distinct SERS signals were observed when the MB concentration was reduced to 10^{-5} M on both the AuNBPs and AuNBPs@TiO_2 substrates, demonstrating the significant signal enhancement enabled by the plasmonic nanostructures. Especially, the AuNBPs@TiO_2 chip exhibited stronger SERS enhancement than the bare AuNBPs substrate. As summarized in Table S1, the mean intensity of the characteristic MB band at 1624 cm^{-1} increased from 20,614 ± 899 for AuNBPs to 28,122 ± 1043 for AuNBPs@TiO_2, corresponding to an enhancement of approximately 36.4%. The corresponding RSD values were 4.36% and 3.71%, respectively, indicating good measurement reproducibility. This enhanced performance can be attributed to the synergistic effect of the AuNBPs@TiO_2 core-shell structure. The AuNBPs core provides strong electromagnetic enhancement through LSPR effect and the localized near fields at their high-curvature tips. Although the TiO_2 shell partially attenuates the plasmonic near field, its dielectric environment, surface adsorption, and possible semiconductor-mediated chemical enhancement may also contribute to the observed SERS response. These results demonstrate that the AuNBPs@TiO_2 chip provides enhanced SERS activity and is suitable for sensitive detection of organic pollutants.

3.5. Sensitivity of AuNBPs@TiO_2 chip

The quantitative analytical performance of the AuNBPs@TiO_2 SERS chip was evaluated using MB solutions with concentrations ranging from 10^{-8} to 10^{-3} M. As shown in Figure 4b, the SERS intensity of the characteristic peak at 1624 cm^{-1} gradually increased with the increasing MB concentration. The calibration curve was established by plotting the SERS intensity at 1624 cm^{-1} against the logarithm of MB concentration. A good linear relationship was obtained with the regression equation of y = 1960.37lgC + 15485.70 and a correlation coefficient of R^2 = 0.9802 (Figure 4c). where C represents the MB concentration in nM. The LOD was calculated according to the formula: LOD = $10^{\frac{y_{blank}+3\sigma-b}{a}}$ where y_{blank} and σ are the mean and standard deviation of the blank response at 1624 cm^{-1} obtained from six measurements, respectively, and a and b are the slope and intercept of the calibration curve, respectively. The measured value of σ was 1975.70, while a and b were 1960.37 and 15,485.70, resulting in a calculated LOD of 3.3 nM. These results demonstrate that the AuNBPs@TiO_2 SERS chip enables sensitive and quantitative detection of trace MB, showing potential for organic pollutant analysis.

3.6. Stability and reproducibility

The signal stability of the AuNBPs@TiO_2 SERS chip was evaluated by collecting SERS spectra from 30 randomly selected sites on the same substrate. As shown in Figure 4d, the intensity distribution exhibited highly uniform signal distribution with no obvious brightness fluctuation, indicating the homogeneous distribution of SERS-active hot spots. The RSD values of the characteristic peaks at 1624 cm^{-1} and 1401 cm^{-1} were 8.24% and 7.97%, respectively (Figure 4e). These results demonstrated the good signal stability and spatial uniformity of the AuNBPs@TiO_2 SERS chip. To further assess

macroscopic uniformity, large-area SERS mapping was performed over a 1 × 1 cm^2 region using a 10 × 10 grid. The intensity map based on the characteristic MB band at 1624 cm^{-1} showed a homogeneous distribution, with an RSD of 8.63% across 100 measurement sites (Figure 4h). Together with the SEM image of the substrate (Figure 4g), these results confirm good spatial uniformity of the drop-cast AuNBPs@TiO_2 chip.

The reproducibility of the AuNBPs@TiO_2 SERS chips was further investigated using six independently prepared chip batches, with three randomly selected sites measured from each batch. SERS spectra were shown in Figure S2. The SERS spectra exhibited highly consistent spectral profiles, with no obvious peak shift for the characteristic peaks at 1624 cm^{-1}. The RSD was calculated to be 5.86% (Figure 4f), indicating good batch-to-batch reproducibility of the fabrication process. All these results demonstrate that the AuNBPs@TiO_2 chip provides reliable and reproducible SERS performance for quantitative MB analysis.

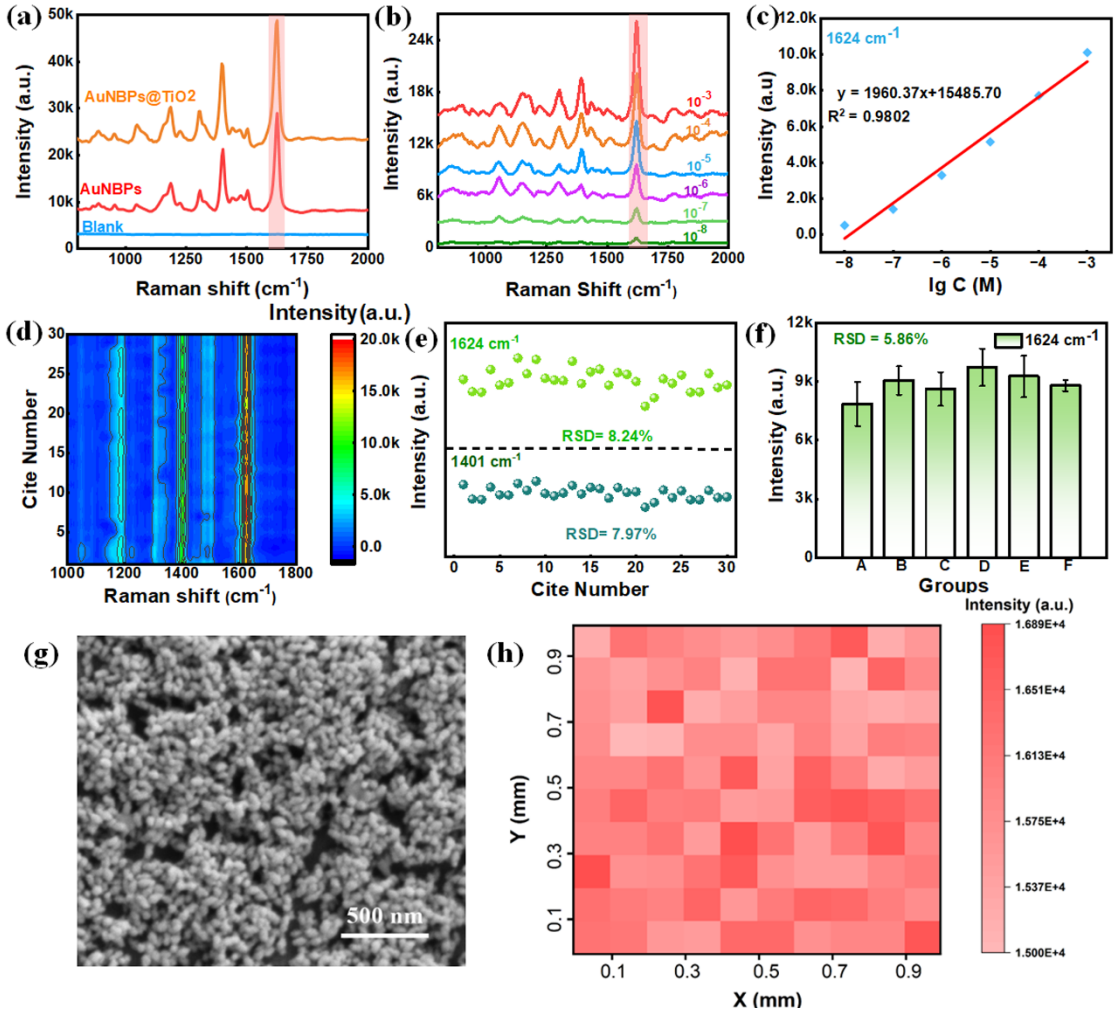

Figure 4. SERS performance of the AuNBPs@TiO_2 chip. **(a)** Raman spectrum of MB without SERS substrate and on AuNBPs and AuNBPs@TiO_2 substrate; **(b)** SERS spectra of MB at different concentrations; **(c)** Calibration curve of the SERS intensity at 1624 cm^{-1} *versus* logarithm of MB concentration; **(d)** SERS signal heatmap obtained from 30 randomly selected sites; **(e)** SERS intensity and corresponding RSD at 1624 cm^{-1} and 1401 cm^{-1}; **(f)** SERS spectra collected from six independently prepared chip batches; **(g)** SEM image of the SERS substrate; **(h)** SERS intensity mapping based on the characteristic MB band at 1624 cm^{-1} over a 1 × 1 cm^2 area.

3.7. In situ monitoring of MB photodegradation

The integration of SERS activity and photocatalytic activity in the AuNBPs@TiO_2 chip enabled real-time *in situ* monitoring of MB photodegradation. As shown in Figure 5a, SERS spectra of 10^{-5} M MB were collected at different irradiation times under xenon lamp irradiation. With increasing irradiation time, the SERS intensity of the characteristic peak at 1624 cm^{-1} gradually decreased, indicating continuous removal of surface-associated MB from the SERS active region. The corresponding SERS intensity at 1624 cm^{-1} was shown in Figure S3. The intensity rapidly decreased to 52% of its initial value after 30 min, further decreased to 21% after 60 min, and reached only 4% after 90 min, demonstrating pronounced time-dependent attenuation of the MB SERS response.

The influence of the initial MB concentration was further investigated using 10^{-4} and 10^{-6} M MB. As shown in Figure 5b,c and Figures S4–S5, the characteristic MB signals progressively decreased under xenon-lamp irradiation for all three concentrations. After 90 min, the SERS signal attenuation reached 95.96%, 98.96%, and 100% for 10^{-4}, 10^{-5}, and 10^{-6} M MB, respectively (Figure 5d), whereas the control without the AuNBPs@TiO_2 chip showed only a 12.3% decrease under the same irradiation conditions. The degradation efficiency increased as the initial MB concentration decreased, which may be attributed to the higher relative availability of photocatalytic active sites and reactive oxygen species for MB molecules at lower concentrations [29]. These results indicate that the AuNBPs@TiO_2 chip effectively promotes MB photodegradation.

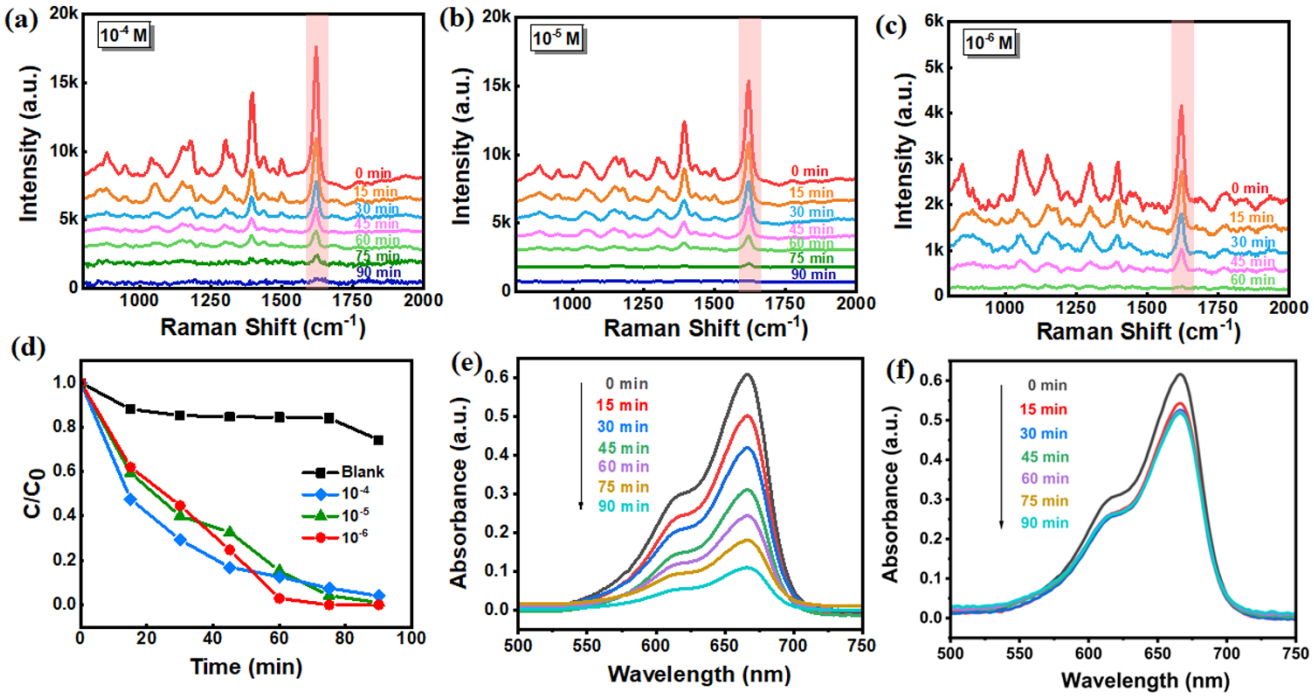

Figure 5. *In situ* SERS monitoring of MB photodegradation. Real-time SERS spectra of **(a)** 10^{-4} M, **(b)** 10^{-5} M, and **(c)** 10^{-6} M MB solution under xenon lamp irradiation; **(d)** The degradation rate curves of MB at different concentrations and the blank sample. UV-vis absorption spectra of 10^{-5} M MB in the presence of AuNBPs@TiO_2 chip **(e)** under xenon-lamp irradiation and **(f)** under dark conditions.

To independently verify MB degradation in the bulk phase, UV-vis absorption spectroscopy was performed under the same xenon-lamp irradiation conditions. As shown in Figure 5e, the characteristic absorption band of MB at approximately 666 nm progressively decreased with irradiation time (Figure 5e), corresponding to an 81.91% decrease after 90 min. The temporal trend was consistent with the signal decrease observed by SERS. In addition, the dark control experiment was performed using the AuNBPs@TiO_2 chip without xenon-lamp irradiation. Only a limited change in MB absorbance was observed (Figure 5f), indicating that the pronounced decrease observed under xenon-lamp irradiation originates from photocatalytic degradation rather than simple desorption. These results suggested that the AuNBPs@TiO_2 chip can serve as a real-time sensing platform for tracking pollutant concentration during photocatalytic degradation.

3.8. Photocatalytic self-cleaning and recycling performance

The photocatalytic self-cleaning cycling capability serves as a key indicator for evaluating the reusability, environmental sustainability, and cost-effectiveness of SERS substrates. The reusability of the AuNBPs@TiO_2 SERS chip was evaluated through repeated MB adsorption, photodegradation and re-adsorption cycles (Figure 6). In each cycle, MB was deposited onto the chip surface and the initial SERS spectrum was recorded as t_0, followed by 90 min of xenon-lamp irradiation and measurement of the residual signal at t_{90}. As shown in Figure 6a, the characteristic peak at t_0 remained clearly visible in each cycle, whereas the signal nearly disappeared after photocatalytic degradation at t_{90}. As shown in Figure 6b, the regenerated chip retained approximately 89.5% of its initial SERS response after eight cycles and approximately 72% after twelve cycles, while the SERS degradation efficiency remained above 90%. The gradual attenuation of the recovered SERS signal may arise from cumulative changes during repeated irradiation and washing, including minor structural rearrangement, incomplete removal of strongly adsorbed species, changes in surface adsorption sites, and alterations in the local plasmonic environment [30]. As summarized in Table S2, although several previously reported self-cleaning SERS substrates exhibit lower detection limits, the AuNBPs@TiO_2 chip provides a competitive combination of quantitative sensitivity, reproducibility, photocatalytic regeneration, and cycling durability.

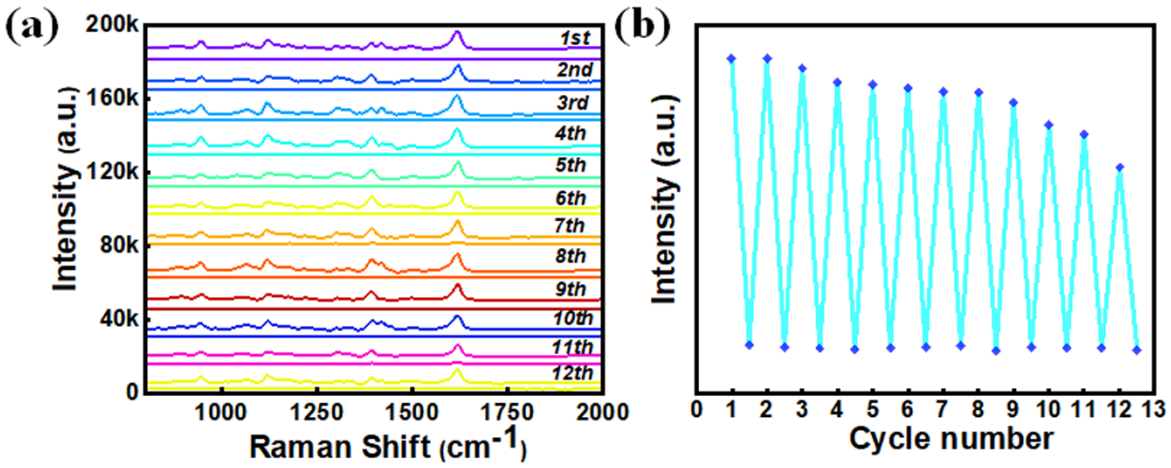

Figure 6. Photocatalytic self-cleaning and recycling performance of the SERS chip. **(a)** SERS spectra after 12 recycling cycles; **(b)** Variation in the SERS intensity at 1624 cm^{-1} with the number of cycles.

3.9. Application in real samples

To further evaluate the practical applicability of the AuNBPs@TiO_2 SERS chip in complex matrices, MB detection was performed in fetal bovine serum (10% FBS in PBS, pH 7.4) and fish muscle samples. MB was spiked at concentrations of 10^{-8}, 10^{-6}, and 10^{-4} M, yielding recoveries of 98.90%–101.68% with RSDs of 2.69%–5.25% in FBS and recoveries of 98.00%–101.91% with RSDs of 1.97%–4.21% in fish muscle samples (Table 1). The satisfactory recoveries and low RSD values indicated that the AuNBPs@TiO_2 SERS chip maintains reliable analytical performance in the presence of complex matrix components, demonstrating the feasibility and reliability of the proposed SERS chip for MB analysis in complex biological and food matrices.

Table 1. Analytical performance of AuNBPs@TiO_2 SERS chip in FBS and fish muscle samples.

Sample	Spiked concentration (μM)	Detected concentration (μM)	Recovery (%)	RSD (%)
FBS	0.01	0.0099	99.00	2.69
	1.00	1.0168	101.68	5.25
	100.00	98.9045	98.90	3.37
Fish muscle	0.01	0.0098	98.00	1.97
	1.00	1.0156	101.56	3.24
	100.00	101.9137	101.91	4.21

4. Conclusion

In this study, a photocatalytic self-cleaning and recyclable AuNBPs@TiO_2 SERS chip was developed for trace detection and *in situ* monitoring of organic pollutant degradation. Uniform AuNBPs@TiO_2 core-shell nanocomposites were prepared by seed-mediated growth and hydrolytic coating of TiO_2, with an optimized TiO_2 shell thickness of approximately 10 nm. Using MB as a model pollutant, the optimized SERS chip exhibited a wide linear range of 10 nM^{-1} mM with a low LOD of 3.3 nM, as well as good uniformity and reproducibility with RSD values below 10%. Moreover, the chip enabled real-time SERS monitoring of MB photodegradation, achieving degradation efficiencies of 95.96%–100% for 10^{-4}–10^{-6} M MB after 90 min of xenon-lamp irradiation. After 12 detection-degradation cycles, the chip retained approximately 72% of its initial SERS response while maintaining a SERS degradation efficiency above 90%, demonstrating good recyclability despite gradual signal attenuation. In addition, satisfactory recoveries obtained in FBS and fish muscle samples further supported the applicability of the platform in complex matrices. The AuNBPs@TiO_2 SERS chip integrates sensitive MB detection, photocatalytic degradation monitoring, and reusable operation within a single platform. These results demonstrate the feasibility of a recyclable plasmonic and photocatalytic SERS platform for coupled detection and degradation monitoring, which provide a recyclable and sustainable SERS analysis.

Data availability statement

The supplementary data supporting this article are available in the online supplementary material. The supplementary contains additional characterization and performance data for the AuNBPs@TiO_2 SERS chip, including reaction-time optimization, inter-batch reproducibility, SERS intensity for the monitoring of MB photodegradation at different concentrations, and Tables for the comparison of SERS responses

between AuNBPs and AuNBPs@TiO_2 substrates, and the comparison with representative self-cleaning SERS substrates.

Declaration of generative AI and AI-assisted technologies

During the preparation of this manuscript, the authors used AI-assisted tool only to improve language and readability. Specifically, the authors used ChatGPT and Grammarly for language polishing only in limited sections of the manuscript. The intellectual content of the manuscript (including ideas, analysis, and conclusion) is original work, and the manuscript complies with academic integrity and publication ethics standards. The authors take full responsibility for the content of the manuscript.

Acknowledgments

This work was financially supported by the National Natural Science Foundation of China (22506057), the Natural Science Foundation of Zhejiang Province (ZCLTGN24B0501, LZ25C200005, LY24B050002), Program for Science and Technology of Jiaxing (2025CGZ042).

Authors' contribution

Conceptualization, Y.Y.; methodology, Y.Y.; formal analysis, J.L., X.F. and A.Y.; investigation, J.L. and X.F.; resources, A.Y. and B.L.; data curation, Y.Y.; writing—original draft preparation, J.L.; writing—review and editing, Y.Y., A.Y. and B.L.; visualization, J.L. and X.F.; supervision, B.L.; project administration, Y.Y. and A.Y.; funding acquisition, Y.Y. All authors have read and agreed to the published version of the manuscript.

Conflicts of interest

Baohong Liu holds the position of Editorial Board Member for *Life Analysis* and has not peer reviewed or made any editorial decisions for this paper. The authors declare no other conflicts of interest.

References

[1] Han X, Rodriguez R, Haynes C, Ozaki Y, Zhao B. Surface-enhanced Raman spectroscopy. *Nat. Rev. Methods Primers* 2021, 1(1):87.

[2] Zhao Y, Kumar A, Yang Y. Unveiling practical considerations for reliable and standardized SERS measurements: lessons from a comprehensive review of oblique angle deposition-fabricated silver nanorod array substrates. *Chem. Soc. Rev.* 2024, 53(2):1004–1057.

[3] Halvorson RA, Vikesland PJ. Surface-enhanced Raman spectroscopy (SERS) for environmental analyses. *Environ. Sci. Technol.* 2010, 44(20):7749–7755.

[4] Li J, Huang Y, Ding Y, Yang Z, Li S, *et al.* Shell-isolated nanoparticle-enhanced Raman spectroscopy. *Nature* 2010, 464(7287):392–395.

[5] Zhu A, Ali S, Jiao T, Wang Z, Xu Y, *et al.* Facile synthesis of fluorescence-SERS dual-probe nanocomposites for ultrasensitive detection of sulfur-containing gases in water and beer samples. *Food Chem*. 2023, 420:136095.

[6] Phan-Quang GC, Lee HK, Phang IY, Ling XY. Plasmonic colloidosomes as three-dimensional SERS platforms with enhanced surface area for multiphase sub-microliter toxin sensing. *Angew. Chem. Int. Ed.* 2015, 127(33):9827–9831.

[7] Zhou P, Zhao C, Song Y, Wang J, He X, *et al.* Semiconductor superlattice with remarkable Raman enhancement for ultrafast culture-free sensing of multiple pathogens. *J. Am. Chem. Soc.* 2026, 148(19):19659–19671.

[8] Li F, Mu X, Tang X, Song X, Sun H, *et al.* Semiconductor SERS on colourful substrates with Fabry-Pérot cavities. *Angew. Chem.* 2023, 62(12):e202218055.

[9] Brus L. Noble metal nanocrystals: plasmon electron transfer photochemistry and single-molecule Raman spectroscopy. *Acc. Chem. Res.* 2008, 41(12):1742–1749.

[10] Alessandri I, Lombardi JR. Enhanced Raman scattering with dielectrics. *Chem. Rev.* 2016, 116(24):14921–14981.

[11] Wang X, Guo L. SERS activity of semiconductors: crystalline and amorphous nanomaterials. *Angew. Chem. Int. Ed.* 2020, 59(11):4231–4239.

[12] Zheng Z, Cong S, Gong W, Xuan J, Li G, *et al.* Semiconductor SERS enhancement enabled by oxygen incorporation. *Nat. Commun*. 2017, 8(1):1993.

[13] Yang L, Peng Y, Yang Y, Liu J, Huang H, *et al.* A novel ultra-sensitive semiconductor SERS substrate boosted by the coupled resonance effect. *Adv. Sci.* 2019, 6(12):1900310.

[14] Liu J, Pan M, Jin J, Lu Y, Feng Z, *et al.* Prepared three-dimensional flowerlike MoS2/Ag@rGO nanocomposite as a self-cleaning SERS substrate for the trace detection of 17β-estradiol in environmental water. *ACS Sustainable Chem. Eng.* 2024, 12(2):893–903.

[15] Arun Kumar KM, Ashok Kumar E, Wang T, Kokulnathan T, Chang Y, *et al.* Ultrasensitive and reusable SERS substrates based on Ag-photodecorated Mn_2O_3 microspheres for nitrofurazone detection. *ACS Sustainable Chem. Eng.* 2023, 11(44):15808–15817.

[16] Zhai Y, Yang H, Zhang S, Li J. Controllable preparation of the Au–MoS_2 nano-array composite: optical properties study and SERS application, *J. Mater. Chem. C* 2021, 9(21):6823–6833.

[17] Li J, Wang Z, Qian L, Zhao J, Zhang Z, *et al.* Hierarchical hotspot engineering for ultrasensitive antibiotics sensing in human body fluids. *Chem. Eng. J.* 2026, 536:175631.

[18] Bontempi N, Cavaliere E, Cappello V, Pingue P, Gavioli L, *et al.* Ag@TiO_2 nanogranular films by gas phase synthesis as hybrid SERS platforms. *Phys. Chem. Chem. Phys.* 2019, 21(45):25090–25097.

[19] Geng Z, Wang G, Gu B, Wen B, Wu Z, *et al.* Machine learning-assisted magnetic nanomotors for the identification and degradation of organic pollutants. *J. Hazard. Mater.* 2025, 499:140078.

[20] Zhu X, Zhuo X, Li Q, Yang Z, Wang J. Gold nanobipyramid-supported silver nanostructures with narrow plasmon linewidths and improved chemical stability. *Adv. Funct. Mater.* 2016, 26(3):341–352.

[21] Campu A, Lerouge F, Chateau D, Chaput F, Baldeck P, *et al.* Gold nanobipyramids performing as highly sensitive dual-modal optical immunosensors. *Anal. Chem.* 2018, 90(14):8567–8575.

[22] Zhang X, Zhang H, Liang H, Yang X, Chai Y, *et al.* Gold nanobipyramid hotspot aggregation-induced surface-enhanced Raman scattering for the ultrasensitive detection of miRNA. *Anal. Chem.* 2023, 95(34):12768–12775.

[23] Pelaez M, Nolan NT, Pillai SC, Seery MK, Falaras P, *et al.* A review on the visible light active titanium dioxide photocatalysts for environmental applications. *Appl. Catal. B* 2012, 125:331–349.

[24] Cowie BE, Porley V, Robertson N. Solar disinfection (SODIS) provides a much underexploited opportunity for researchers in photocatalytic water treatment (PWT). *ACS Catal.* 2020, 10(20):11779–11782.

[25] Fu A, Chen X, Tong L, Wang D, Liu L, *et al.* Remarkable visible-light photocatalytic activity enhancement over Au/p-type TiO_2 promoted by efficient interfacial charge transfer. *ACS Appl. Mater. Interfaces* 2019, 11(27):24154–24163.

[26] Guerrero-Araque D, Sierra-Uribe JH, Camposeco R, Romero R, Gómez R *et al.* Accelerated transfer and separation of charge carriers during the photocatalytic production of hydrogen over Au/ZrO_2–TiO_2 structures by interfacial energy states. *Int. J. Hydrogen Energy* 2023, 48(42):15956–15966.

[27] Wustholz KL, Henry AI, McMahon JM, Freeman RG, Valley N, *et al.* Structure−activity relationships in gold nanoparticle dimers and trimers for surface-enhanced Raman spectroscopy, *J. Am. Chem. Soc.* 2010, 132(31):10903–10910.

[28] Wang P, Krasavin AV, Liu L, Jiang Y, Li Z, *et al.* Molecular plasmonics with metamaterials. *Chem. Rev.* 2022, 122(19):15031–15081.

[29] Wu B, Liu D, Mubeen S, Chuong TT, Moskovits M, *et al.* Anisotropic growth of TiO_2 onto gold nanorods for plasmon-enhanced hydrogen production from water reduction. *J. Am. Chem. Soc.* 2016, 138(4):1114–1117.

[30] Lee T, Bui HT, Yoo J, Ra M, Han SH, *et al.* Formation of TiO_2@carbon core/shell nanocomposites from a single molecular layer of aromatic compounds for photocatalytic hydrogen peroxide generation. *ACS Appl. Mater. Interfaces* 2019, 11(44):41196–41203.